NON-DIMENSIONAL ANALYSIS OF A HUDIMIFICATION-DEHUMIDIFICATION SYSTEM DRIVEN BY PV/T COLLECTORS FOR DESALINATE WATER PRODUCTION

Riccardo Simonetti, Luca Molinaroli and Giampaolo Manzolini
Department of Energy, Politecnico di Milano, Via Lambruschini 4, 20156 Milano, (Italy)

Summary

This work summarizes a non–dimensional performance analysis of a small-scale humidification-dehumidification system (HDH) driven by hybrid photovoltaic-thermal (PV/T) solar collectors for water desalination. A model was developed to the optimal working conditions in a generalized formulation, starting from the effectivenesses of the components and the operating parameters, namely the feed water to air mass flow rate ratio (MR) and the fresh water to feed water mass flow rate recovery ratio (RR).

Keywords: HDH, Solar Desalination, Performance Analysis

1. Introduction

The constant growth of the population and the expansion of the global economy, in particular in developing countries, are driving up the demand of energy, water, and food. It is expected that the demand for energy will nearly double by 2050, and the one of water and food will increase by over 50 % (IEA, 2018; IRENA, 2015). Desalination is the most energy-intensive water production process available today. It consumes at least 75.2 TWh of electricity per year and most of the energy required for desalination is supplied by fossil fuels. The capacity that rely on renewables is less than 1 % of the total installed capacity (IRENA, 2015). For relatively small-decentralized community, the humidification-dehumification (HDH) cycle is a promising technology thanks to a low environmental and social impact through the possible integration with a renewable energy source (Gabrielli et al., 2019). HDH process can operate at low temperatures, requires a low-level technological features and low maintenance, hence is more appropriate for cases where technical support is limited (Zubair et al., 2017). A great variety of configurations are proposed in literature to improve the performance of the system: multistage asset (Wu et al., 2017), multiple injections (Thiel et al., 2013), direct contact dehumidifier (He et al., 2017), coupling with a heat pump (Srithar and Rajaseenivasan, 2018), heat recovery (Zubair et al., 2018), variation of air pressure (Rahimi-Ahar et al., 2018). In all these cases, identifying the optimal sizing and operating conditions is the main challenge as performance of different configurations must be consistently analyzed and compared. Performance of HDH system is normally evaluated in literature through the definition of some parameters (Prakash Narayan et al., 2010), for example the heat capacity ratio (HCR) and the enthalpy pinch point (ψ). According to the authors' opinion, these are not fully representative of the technology potentialities. For example, the maximum temperature of the cycle (T_3 in Figure 1) is a common constrain, which limits the selection of the heat source for the cycle. The scope of this work is to propose a general analysis of closed-air open-water (CAOW) HDH cycles based on non-dimensional performance, independently from the heat source and components adopted.

The developed model is based on the components performance (effectiveness) and system operating parameters, namely the feed water to air mass flow rate ratio (MR) and the fresh water to feed water mass flow rate recovery ratio (RR). A sensitivity analysis is carried out to evaluate the influence of these variables on the performance of the whole system. After this analysis, an example of the model application for preliminary sizing of the two columns and the PV/T solar field is performed.

The paper is structured as follow. Section 2 describes the concept of the HDH system. Section 3 presents the model description and the non-dimensional equation rearrangement. In Section 4, results are presented and discussed. Finally, Section 5 draws the conclusions of the work pointing out future research activities.

doi:10.18086/swc.2019.46.04 Available at http://proceedings.ises.org

2. Concept

The concept of the system is based on the humidification-dehumidification (HDH) process, in the closed air-open water (CAOW) version of the cycle, shown in Figure 1.

A seawater flow $\dot{m}_{sw}$ is pre-heated in the dehumidifier that consists of a finned tube heat exchanger. The seawater is further heated (in this work using PV/T collectors), and then is sprayed in the humidifier. The humidifier is a direct-contact column where the seawater is counterflow to air stream $\dot{m}_{da}$ where a simultaneous heat and mass transfer occurs. The seawater cools down and evaporates, with the concentrated seawater ending in the $\dot{m}_{brine}$ discharged from the humidifier, whereas the air is heated and humidified. Afterwards, the air flows inside the dehumidifier, where it is cooled below its dew-point temperature and the pure water $\dot{m}_{pw}$ is produced. Finally, the air stream flows back to the humidifier, closing the loop.

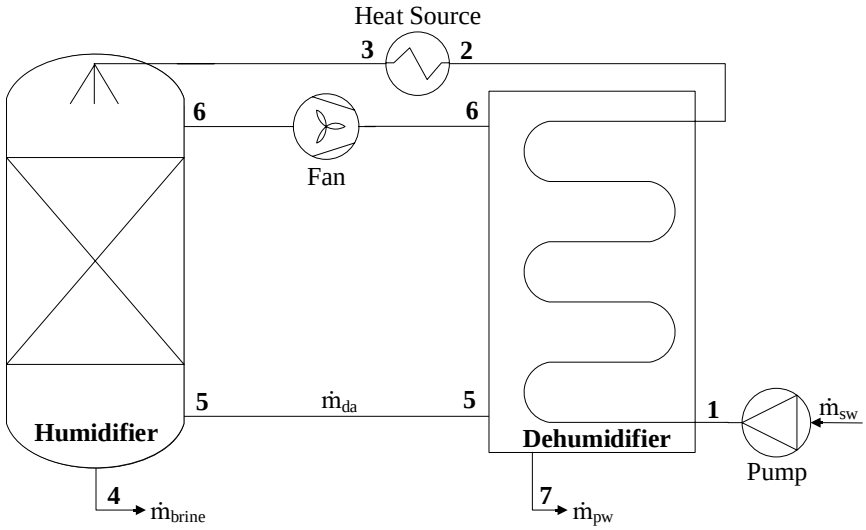

Figure 1 - Schematic of a closed-air open-water HDH process

3. Model Description

The analysis of the HDH system in general terms requires the description of the components as black boxes. Firstly, mass balances are taken into account, as shown in the following equations:

$$\dot{m}_{pw} = \dot{m}_{da} \cdot (\omega_6 - \omega_5) \quad (1)$$

$$\dot{m}_{brine} = (\dot{m}_{sw} - \dot{m}_{pw}) \quad (2)$$

Secondly, energy balances of the dehumidifier and humidifier are considered too, as follow:

$$\dot{Q}_{de} = \dot{m}_{sw} \cdot h_2 - \dot{m}_{sw} \cdot h_1 = \dot{m}_{da} \cdot h_6 - \dot{m}_{da} \cdot h_5 - \dot{m}_{pw} \cdot h_7 \quad (3)$$

$$\dot{Q}_{hu} = \dot{m}_{sw} \cdot h_3 - \dot{m}_{brine} \cdot h_4 = \dot{m}_{da} \cdot h_6 - \dot{m}_{da} \cdot h_5 \quad (4)$$

Finally, the humidifier and the dehumidifier are described by their effectivenesses, as shown in the following equations:

$$\varepsilon_{de} = \frac{\dot{Q}_{de}}{\dot{Q}_{de,max}} = \frac{\dot{Q}_{de}}{\min(C_{sw}, C_{da}) \cdot (T_6 - T_1)} \quad (5)$$

$$\varepsilon_{hu} = \frac{\dot{Q}_{hu}}{\dot{Q}_{hu,max}} = \frac{\dot{Q}_{hu}}{\min(C_{sw}, C_{da}) \cdot (T_3 - T_5)} \quad (6)$$

To simplify the model resolution, the moist air is assumed as saturated consistently with other approaches available in literature (Gabrielli et al., 2019). Moreover, the temperature of the fresh water produced is considered equal to the air temperature at the outlet of the dehumidifier.

The resulting non-dimensional equations based on the mass flow rate ratio (MR) and the recovery ratio (RR) which are the representative operating parameters of the HDH cycle are as follow:

$$MR = \frac{\dot{m}_{sw}}{\dot{m}_{da}} \tag{7}$$

$$RR = \frac{\dot{m}_{pw}}{\dot{m}_{sw}} \tag{8}$$

They are obtained rearranging the set of equations previously described pointing out the possibility to study the system in a general form so to easily find the optimal working conditions. Equations (9) to (11) summarize the non-dimensional rearrangement:

$$\varepsilon_{de} = MR \cdot \frac{T_2 - T_1}{\min\left(MR, c^*_{p,de}/c_{p,sw}\right)\cdot(T_6 - T_1)} \tag{9}$$

$$\varepsilon_{hu} = MR \cdot \frac{T_3 - (1-RR)\cdot T_4}{\min\left(MR, c^*_{p,hu}/c_{p,sw}\right)\cdot(T_3 - T_5)} \tag{10}$$

$$MR = \frac{h_6 - h_5 - MR\cdot RR\cdot h_7}{h_2 - h_1} = \frac{h_6 - h_5}{h_3 - (1-RR)\cdot h_4} = \frac{\omega_6 - \omega_5}{RR} \tag{11}$$

where c_p^* is the fictitious isobaric specific heat capacity of the moist air and it is evaluated as the ratio of the variation of the enthalpy of the saturated moist air and the variation of the wet bulb temperature. The following equation explains the calculation of c_p^*:

$$c_p^* = \frac{h(T+\delta) - h(T-\delta)}{2\delta} \tag{12}$$

where δ is small number. In this analysis, a value of 1 °C is used.

4. Results

The performance of the HDH system are described in terms of the gained output ratio (GOR), which is expressed by the following equation (Mistry et al., 2010):

$$GOR = \frac{\dot{Q}_{evap}}{\dot{Q}_{source}} = \frac{\dot{m}_{pw}\cdot\Delta h_{l-v}}{\dot{m}_{sw}\cdot(h_3 - h_2)} = RR \cdot \frac{\Delta h_{l-v}}{(h_3 - h_2)} \tag{13}$$

Results are shown in Figure 2, where the GOR is plotted as function of RR and MR, with both the effectivenesses of the humidifier and the dehumidifier set equal to 0.8. For each RR exists a MR that maximizes the GOR. This behavior is consistent with previous work available in literature (Mistry et al., 2010). On the left side of this curve, the GOR reduces as consequence of the lower heat capacity of the seawater flow at lower MR. The lower heat capacity limits the evaporation of water into the air, therefore, a higher thermal power is required by the heat source to maintain the RR constant, consequently reducing the GOR.

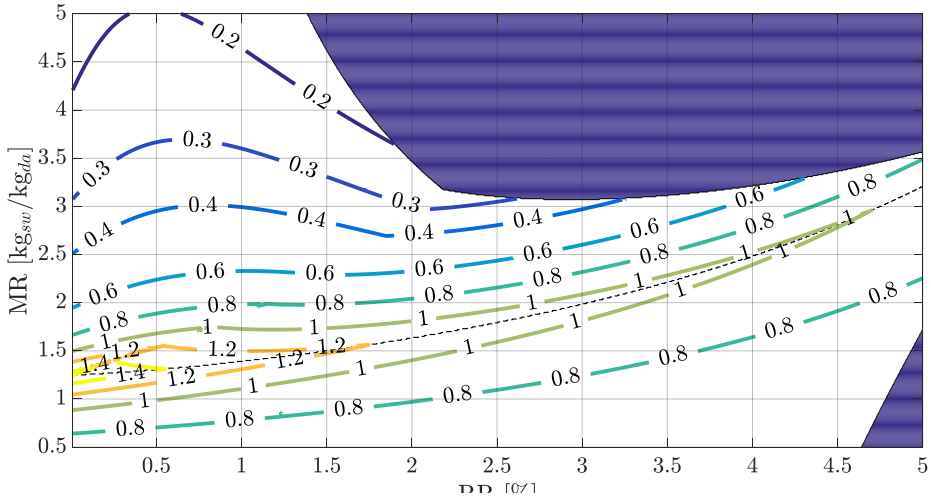

Figure 2 - Representation of GOR of the HDH cycle as a function of MR and RR

On the other hand, increasing the MR from the optimum value changes the minimum heat capacity from the seawater to the air in the humidifier (where the fictitious isobaric specific heat capacity of the moist air is lower because the temperature is lower at the inlet of the column). Therefore, the RR can be kept constant increasing the temperature difference done by the heat source, reducing the GOR. As happen in a standard counter-flow heat exchanger, the optimal condition occurs when the heat capacities of the two flow coincide.

At higher RR, the maximum GOR reduces: in order to produce more fresh water, a higher temperature difference is necessary across the humidifier and dehumidifier. Moreover, the optimal point shift towards higher MR because of the increased fictitious specific heat capacity of the air consequence of the higher temperature of the air cycle. This behavior is highlighted with the black dashed line in the graph. Finally, the two yellow-filled areas represent conditions where the HDH system reaches very high temperature, above 100 °C, meaning that the solution is not feasible as the considered system cannot operate.

Figure 3 shows the maximum temperature T_3 of the HDH cycle varying MR and RR. Consistently with the behavior of the GOR, T_3 has a minimum where the GOR is maximum and increase with the RR. For a HDH system with PV/T panels as the heat source, the preferable configuration is the one with the lowest temperature, as consequence of the low thermal efficiency of this technology at high temperatures. As the optimal configuration occurs with the maximum GOR, it can be stated that the HDH plus PV/T system can be a promising and efficient way to couple these technologies. The reason of the two non operating zones is better explained in this graph, because is clearly visible the overcoming of the boiling temperature of the water.

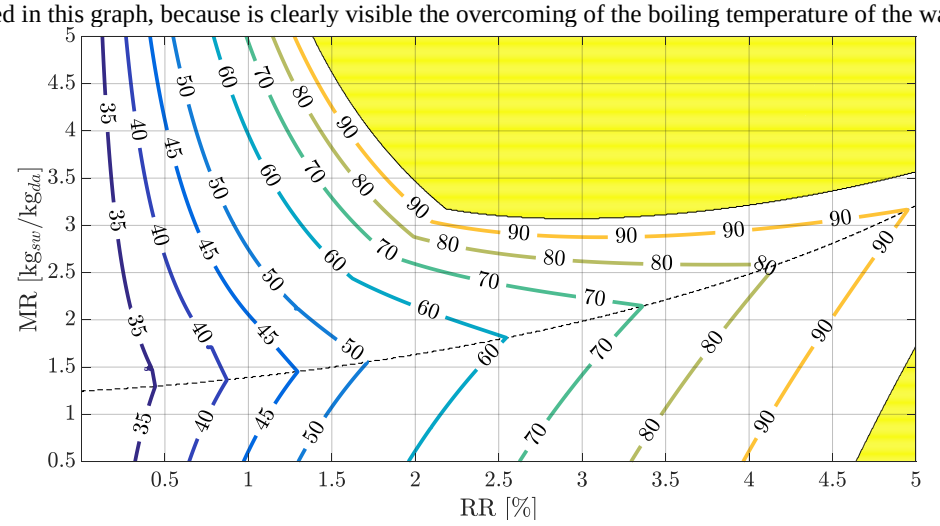

Figure 3 - Representation of the maximum temperature of the HDH cycle as a function of MR and RR

In Figure 4, the temperature difference across the thermal source is described as a function of RR and MR. The trend is the very similar to the one of the maximum temperature T_3. With low RR the temperature difference is very low (i.e. below 5 °C) which is an advantage for the coupling with the PV/T panels.

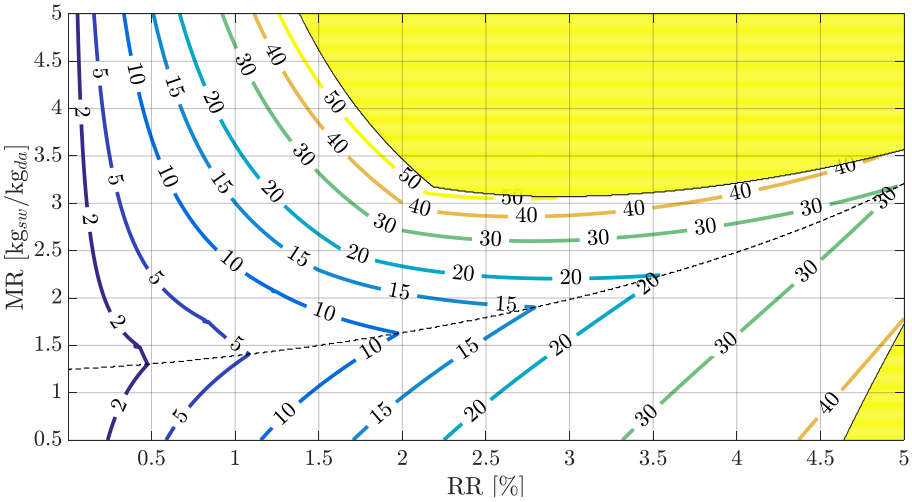

Figure 4 - Representation of the source temperature difference of the HDH cycle as a function of MR and RR

Figure 5 presents the GOR as a function of the inlet seawater temperature and the MR. Results shows that the higher the temperature the higher is the GOR, because of the increasing slope of the saturation curve. In fact, a lower air temperature increase is needed to achieve the same humidity ratio, and consequently a lower temperature increase from the thermal source, leading to higher performance. The MR that maximize the GOR increases as the seawater temperature increases, as all the HDH cycle temperatures shift up: higher seawater inlet temperature leads to higher fictitious specific heat capacity, and increases the MR to reach the balance of the heat capacities of the two flows in the humidifier.

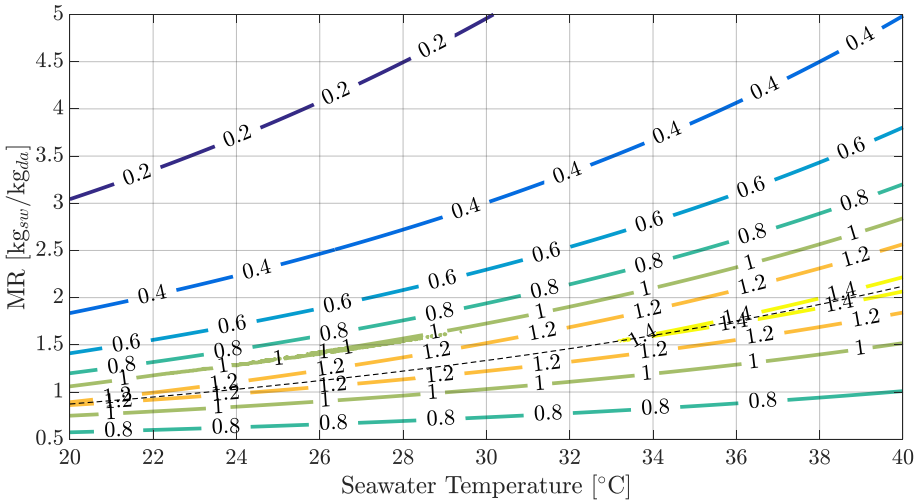

Figure 5 - Representation of the GOR of the HDH cycle as a function of MR and the seawater temperature

For completeness, an analysis varying the effectivenesses of the humidifier and dehumidifier was performed (see Figure 6). Increasing the performance of the two columns can increase the GOR up to three times. Therefore, it is obvious that in the design of the system, the effectivenesses of these two components have to be as high as possible, so to maximize the performance and minimize the operating costs. Moreover, the additional investment costs of the HDH system can be even fully balanced by the cost reduction of the solar field. Higher performance of the two columns reduces the temperature difference by the thermal source reducing the number of PV/T panels installed, with account for the higher share of the investment cost in a HDH cycle (Gabrielli et al., 2019). The sizing optimization of the HDH system will be performed in a future work.

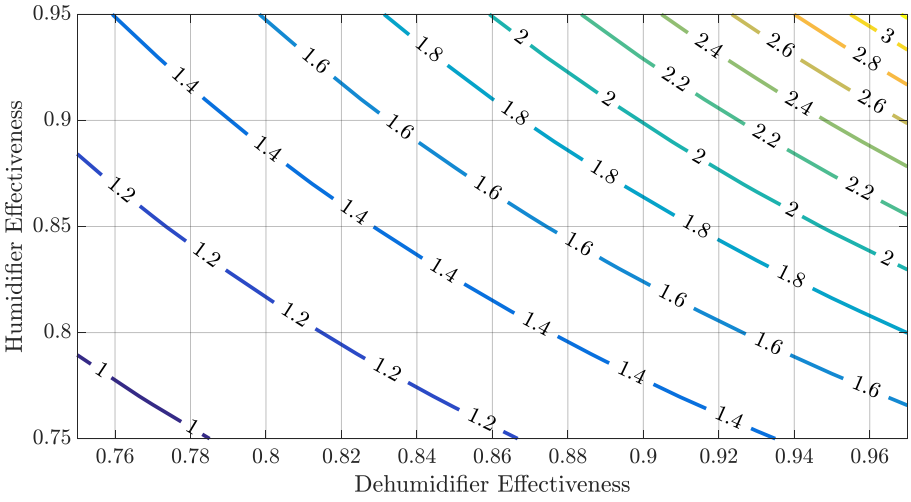

Figure 6 - Representation of the GOR of the HDH cycle as a function of the effectivenesses of humidifier and dehumidifier

Another analysis that can be done looking at the previous graph is that the GOR increases more rapidly with the increasing of the dehumidifier effectiveness respect to the humidifier one. This is simply explained considering that in the dehumidifier the fresh water is produced, so higher is the column performance and higher the water production, which influences directly the GOR (eq. 13).

Finally, the validity of the non-dimensional analysis discussed so far is demonstrated by its application for the preliminary sizing of a HDH system with PV/T panels. Models of the direct-contact humidifier and the finned tubes dehumidifier and characteristics of commercial PV/T panels (SoLink, 2018) were used to find the geometry of the columns and the area of the solar field. All the models' description ad sizing procedure are discussed in another ongoing work. The productivity of the system was assumed equal to 50 kg/h of fresh water, with 650 W/m² of solar irradiance and 30 °C of ambient temperature. Moreover, three different values of effectivenesses were assumed, equal for the two columns, in order to analyze the influence of these parameters on the system sizing. Details of the sizing are summarized in Table 1.

Table 1 - Main results of the HDH system sizing for three different columns' effectivenesses

	Performance			PV/T	Dehumidifier		Humidifier [m]		Auxiliary [kW]		Production [kW]	
ε_D | ε_H	MR	RR [%]	GOR	Panels	Tubes	Rows	Diameter	Height	Fan	Pump	Electricity	Heat
0.75	1.329	0.55	1.10	77	89	14	0.71	3.3	2.35	1.42	11.4	31.8
0.85	1.327	0.80	1.76	52	61	22	0.58	5.3	2.35	0.97	7.7	19.8
0.95	1.331	1.21	3.10	35	40	37	0.47	9.7	2.54	0.66	5.0	11.3

In addition to the GOR increase with the effectivenesses of the dehumidifier and humidifier, it is possible to notice that the number of PV/T panels halving from 0.75 to 0.95. Moreover, also the number of frontal tubes in the humidifier decreases, due to the lower air mass flow rate circulating in the cycle. The number of rows obviously increases as the effectiveness does. The same considerations can be extended to the humidifier dimensions. Focusing on the auxiliaries consumptions, the increase of the RR and the invariance of the MR have therefore a lower flow rates. Thus, the pump consumption is reduced while the fan one remains roughly constant due to higher pressure drops. Finally, looking at the productions, the electricity produced reduces proportionally with the PV/T modules, and in the same way, the heat produced does.

5. Conclusions

In this paper, a non-dimensional analysis of a HDH system was carried out. Starting from mass and energy balances and considering the effectivenesses of the humidifier and dehumidifier, all the thermodynamic conditions of the cycle were identified. Then, introducing the operating parameters MR and RR, the equations were rearranged to generalize the system performance only as a function of the MR and RR and the two components' effectiveness.

Results have shown that for each value of RR exists a MR that maximizes the performance parameter GOR, which corresponds to equal heat capacities of the two flows in the humidifier. Moreover, the higher the RR the higher is the MR, due to the increasing of the temperature of the cycle, but this penalizes the GOR. The maximum temperature of the cycle presents a minimum related to the GOR behavior, and for low RR the temperature needed can be even lower than 40 °C, which is an advantage for coupling this system with PV/T technology. An analysis at different columns effectiveness was performed underlining the importance of the performance of these two components, especially the dehumidifier one. Finally, operating at very high GOR can reduce both the operating and investment costs thanks to the smaller solar field area consequence of the reduction of the temperature difference required by the heat source.

The analysis of the results of the sizing method have shown the influence of the effectiveness of the two columns, where with a higher value it is associated higher number of dehumidifier rows and humidifier height, but in opposition a lower number of PV/T panels, dehumidifier frontal tubes and humidifier diameter.

The introduction of the investment costs in a future work will allow the optimization of the components sizing in economic terms.

6. References

Gabrielli, P., Gazzani, M., Novati, N., Sutter, L., Simonetti, R., Molinaroli, L., Manzolini, G., Mazzotti, M., 2019. Combined water desalination and electricity generation through a humidification-dehumidification process integrated with photovoltaic-thermal modules: Design, performance analysis and techno-economic assessment. Energy Convers. Manag. X 1, 18. https://doi.org/10.1016/j.ecmx.2019.100004

He, W.F., Huang, L., Xia, J.R., Zhu, W.P., Han, D., Wu, Y.K., 2017. Parametric analysis of a humidification dehumidification desalination system using a direct-contact dehumidifier. Int. J. Therm. Sci. 120, 31–40. https://doi.org/10.1016/j.ijthermalsci.2017.05.027

IEA, 2018. World Energy Outlook.

IRENA, 2015. Renewable Energy in the Water, Energy and Food Nexus.

Mistry, K.H., Lienhard V, J.H., Zubair, S.M., 2010. Effect of entropy generation on the performance of humidification-dehumidification desalination cycles. Int. J. Therm. Sci. 49, 1837–1847. https://doi.org/10.1016/j.ijthermalsci.2010.05.002

Prakash Narayan, G., Mistry, K.H., Sharqawy, M.H., Zubair, S.M., Lienhard V, J.H., 2010. Energy effectiveness of simultaneous heat and mass exchange devices. Front. Heat Mass Transf. 1. https://doi.org/10.5098/hmt.v1.2.3001

Rahimi-Ahar, Z., Hatamipour, M.S., Ghalavand, Y., 2018. Solar assisted modified variable pressure humidification-dehumidification desalination system. Energy Convers. Manag. 162, 321–330. https://doi.org/10.1016/j.enconman.2018.01.063

SoLink, 2018. PV/T SoLink [WWW Document]. URL https://www.solink.it/download/209/ (accessed 1.28.19).

Srithar, K., Rajaseenivasan, T., 2018. Recent fresh water augmentation techniques in solar still and HDH desalination – A review. Renew. Sustain. Energy Rev. 82, 629–644. https://doi.org/10.1016/j.rser.2017.09.056

Thiel, G.P., Miller, J.A., Zubair, S.M., Lienhard, J.H., 2013. Effect of mass extractions and injections on the performance of a fixed-size humidification-dehumidification desalination system. Desalination 314, 50–58. https://doi.org/10.1016/j.desal.2012.12.025

Wu, G., Zheng, H.F., Wang, F., Chang, Z.H., 2017. Parametric study of a tandem desalination system based on humidification-dehumidification process with 3-stage heat recovery. Appl. Therm. Eng. 112, 190–200. https://doi.org/10.1016/j.applthermaleng.2016.10.078

Zubair, M.I., Al-Sulaiman, F.A., Antar, M.A., Al-Dini, S.A., Ibrahim, N.I., 2017. Performance and cost assessment of solar driven humidification dehumidification desalination system. Energy Convers. Manag. 132, 28–39. https://doi.org/10.1016/j.enconman.2016.10.005

Zubair, S.M., Antar, M.A., Elmutasim, S.M., Lawal, D.U., 2018. Performance evaluation of humidification-dehumidification (HDH) desalination systems with and without heat recovery options: An experimental and theoretical investigation. Desalination 436, 161–175. https://doi.org/10.1016/j.desal.2018.02.018